Report
R-15-02
February 2017

Solute transport in channel networks with radial diffusion from channels in a porous rock matrix

Ivars Neretnieks

SVENSK KÄRNBRÄNSLEHANTERING AB

SWEDISH NUCLEAR FUEL
AND WASTE MANAGEMENT CO

Box 250, SE-101 24 Stockholm
Phone +46 8 459 84 00
skb.se

SVENSK KÄRNBRÄNSLEHANTERING

ISSN 1402-3091
SKB R-15-02
ID 1486489

February 2017

Solute transport in channel networks with radial diffusion from channels in a porous rock matrix

Ivars Neretnieks

Department of Chemical Engineering
Royal Institute of Technology, KTH

Keywords: Channelling, Channel networks, Fracture networks, Radial diffusion in rock matrix, Retardation.

Abstract

Flow and advective solute transport in fractured rock takes place in channels in fractures. In two detailed site investigations in granitic rock in Sweden made to find a suitable site for the Swedish final repository for spent nuclear fuel it was found that of intersected fractures in dozens of core drilled boreholes down to 1 000 m only 2–3 % of the fracture intersections were hydraulically conductive. The information has been used to build fracture network models assuming that flowing fractures are fully open over their entire extent. Because many of the conducting fractures are large compared to the diffusion penetration depth the matrix diffusion is modeled to be orthogonal to the fracture surface. This is not realistic. Field observations show that water flows in narrow, less than 0.3 m wide channels. For narrow channels the diffusion would increasingly become radial as the penetration depth by diffusion becomes larger than the channel width. With radial diffusion the rate of uptake into the matrix is much faster that by linear diffusion. To find the same intensity of flowing channels in boreholes these must lie much closer to each other than fully conducting fractures. With radial diffusion the rock matrix between channels is more rapidly accessed by the solutes.

In combination with the fact that narrow channels must form a much denser network of channels than wide channels (entirely open fractures) for a given intensity of flow wetted surface, FWS, in the rock, the water in the porous rock matrix between the channels much more rock is accessed by diffusion. This leads to much larger retardation of solutes carried by the seeping water.

In some examples based on field data it is shown that even a non-sorbing nuclide such as the very long-lived ^{129}I can be retarded very strongly. The shorter lived ^{14}C could decay by many orders of magnitude, which would not be the case if diffusion is linear from the channels. Sorbing nuclides are even more strongly retarded. This can have a considerable impact in a safety analysis for a nuclear waste repository.

The novelty of this report is that the presence of narrow channels will give radial diffusion when the diffusion penetration depth becomes comparable to the channels width. The network of narrow channels is much denser than one with wide channels (entire fracture widths as used in fracture networks), which with radial diffusion results in a vastly increased fraction of rock mass reached by the diffusing solutes because radial diffusion from the channels is much more space filling than linear diffusion from the same channels. It is the combination of dense channels networks and radial diffusion that causes the dramatic increase of retardation.

Contents

1 Background and introduction

In some countries high-level nuclear waste will be deposited deep in crystalline rocks. Crystalline rocks contain fractures, which play an important role in understanding and modelling water flow and solute transport. In fractured rocks water flows mainly in fractures because the rock matrix has a very low hydraulic conductivity. However, the low permeability porous rock matrix plays a dominating role for solute transport role because solutes can diffuse in and out of the stagnant water in the matrix and gain access to a much larger water volume and more crystal surfaces to react with than in the flowing fractures (Neretnieks 1980). The rock matrix pore water can delay the transport of solutes and allow many radioactive contaminants to decay to negligible values. In most papers on modelling flow and transport in fractures where matrix diffusion is important it is assumed that the diffusion is one-dimensional and is orthogonal to the fracture surface. This paper explores the impact on the solute transport and retardation of radial diffusion from narrow channels in fractured rock.

Discrete fracture network models, DFN, have been used to model large-scale flow and transport in granitic rock (e.g. Cacas 1990 a, b, Joyce et al. 2010, Hartley and Roberts 2013). Theoretical and computational approaches are described by Sahimi (2011). An overview of earlier work can be found in Berkowitz (2002). In fracture networks models the conducting fractures are modelled as being fully open over their entire extent. The fractures intersect each other forming the conductive network. Each fracture is then assigned a volume, size and transmissivity, taken from some stochastic distribution (Dershowitz and Fidelibus 1999). A considerable number of papers on network modelling are referenced in Neuman (2005) who also gives an overview of the difficulties and intricacies encountered in modelling flow and transport in fractured media. An overview of groundwater flow modelling of a Swedish site is reported in Selroos and Follin (2010). Solute transport processes, matrix diffusion and other processes in fractured rock can be found in and SKB (2004).

The transmissivity distribution can be experimentally assessed by injecting or withdrawing water at different locations in drilled boreholes in the rock mass. This can be done by sealing off narrow parts of the borehole and injecting/withdrawing water or can by changing the hydraulic head in the entire borehole and measuring the inflows at different locations by some flowrate-metering device. Different such tools are available. Borehole cameras are used to inspect the hole and locate the flowing and non-flowing fractures. Cores from the boreholes are also inspected and give information on which fractures are open, partly closed or closed and their orientations. The closed fractures are considerably more abundant that the open and partly open fractures. However, far from all the latter are found to be transmissive. The fraction of transmissive fractures in some well-investigated granitic rock masses were found to make up a few percent of all fractures in the boreholes (Rhén et al. 2008, Follin 2008). Fracture size distributions are assessed from measurements on outcrops but it is recognized that this may not be representative of the fractures at depth. Fracture apertures are estimated from the measured hydraulic transmissivities by the so-called cubic law but with modifications based on observations that the “hydraulic” aperture is often considerably smaller than the physical aperture.

The assumption that fractures are either open or closed is unrealistic and introduces further uncertainties in fracture network modelling. Fractures in rock under stress must be in contact in places to transmit the stress and can be open in some locations where the two fracture faces do not exactly fit. The misfit can be caused by dis-alignments induced when the fracture formed or later when tectonic movement sheared the fractures. Where open locations connect over large distances, hydraulically connected paths exist that may carry water. For a given hydraulic gradient-direction preferential flowpaths form. With a different gradient direction the water seeks out other paths. We call such paths channels but acknowledge that these are mostly not permanent physical channels although such may form by dissolution/precipitation of the rock minerals over long time.

Channelling has been observed in small scale laboratory experiments in a few cm to tens cm samples with natural or induced fractures, in large laboratory experiments, in field experiments over meters to 100s of meters and on walls of drifts and tunnels where water is seen to emerge in less than cm to tens of cm wide channels in the otherwise non-seeping fracture. Tsang and Neretnieks (1998) give an overview of a large number of experiments in which channelling is observed, conceived and interpreted. Bodin et al. (2003 a, b) discuss the fundamental mechanisms of flow and transport in

fractures and Cvetkovic et al. (1999) discuss transport of reactive solutes in a single fracture. Crawford (2008) reports a number of cross-hole experiments and single well injection withdrawal experiments that have been evaluated using channelling assumptions. Channel widths of centimetres and larger were reported but it is noted that there are considerable uncertainties in the interpretations.

Many papers on simulation of flow and solute transport in variable aperture fractures have been published, some based of measured data from real fractures, others based on general assumptions on local transmissivity variations and correlation lengths. Particle tracking is often used to find the flowpaths (Tsang and Tsang 1987, 2001, Tsang et al. 1988, Moreno et al. 1990). Also analytical methods have been developed to do this (Amadei and Illangasekare 1994). Commonly it is found that one or a few paths carry by far the largest fraction of the water flow through the fracture. It is also found that breakthrough curves often have multiple peaks, which suggests that there are several more or less independent flowpaths.

Solutes that are carried by the water in channels in fractures will interact with the rock matrix in several ways. The solutes may diffuse in and out of the porous rock matrix accessing the stagnant water and therefore becoming diluted and retarded. Sorbing solutes sorb on the inner surfaces of the rock matrix. The rock may be altered near the fracture and the fracture surfaces may be covered with different mineral coatings, which will influence the access to the matrix (Mahmoudzadeh et al. 2014). They may also diffuse in and out of stagnant water in parts of the fracture adjacent to the channel where flow is so slow that flow velocity can be neglected. This has a similar effect as the diffusion in and out of the rock matrix adjacent to the channel and contributes to deplete solute in the flowing water in the channel (Neretnieks 2006). Johns and Roberts (1991) modelled the transport in and between two adjacent flowing channels with different velocities. The solute that enters the stagnant or slowly seeping water will come in contact with more fracture surface into which it can diffuse. These processes additionally dilute and retard the solute.

Sorbing solutes such as positively charged ions, e.g. many radionuclides, when entering the rock matrix have access to the negatively charged inner surfaces of the matrix on which they sorb. This can lead to considerable increase of the retardation. The diffusion into stagnant zones in the fracture adjacent to the channel can be accounted for in channel network but not in fracture network models because of the assumption of fully transmissive or fully closed fractures. Diffusion into stagnant zones outside the channel will increase the surface from which matrix diffusion occurs and additionally retard the solute.

Matrix diffusion from fractures in networks has been modelled and incorporated in radionuclide chain transport codes (Joyce et al. 2010, Hartley and Roberts 2013). However, these studies are based on the concept that fractures are either open or closed over the entire fracture with the consequences that the flowing fractures are very sparse and that the rock between and far from the fractures is not readily accessible by molecular diffusion during times of interest. The sparse fractures may lead to poor connectivity of the fracture network and can be sensitive to fracture size distribution as has been pointed out by Berkowitz (2002). The fracture size distribution, assessed from observation on outcrops, has a considerable influence on the connectivity of the fracture network. The long distance between fractures and resulting limited matrix access may lead to underestimation of solute retardation. Poor connectivity in the fracture network on the other hand may lead to overestimation of isolation power of the rock mass.

There are many observations that flow in fractures is channelized. This has been observed in laboratory scale fractures (Neretnieks et al. 1982, Moreno et al. 1985, 1988, Brown et al. 1998, Huber et al. 2012, Develi and Babadagli 2015). There are also observations on larger scales that show distinct channelling (Abelin et al. 1983, 1985). There are observations in large field experiments as well as on rock faces in drifts and tunnels (Abelin et al. 1991, 1994, Birgersson et al. 1992, 1993, Tsang and Neretnieks 1998, Pamquist and Stanfors 1997, Stober and Bucher 2006). It is also found that many of the channel intersections themselves can conduct water (Abelin et al. 1991). An example of channelling in granitic rock from in the Bolmen tunnel in Sweden (Stanfors 1997), is shown in Figure 1-1. In the granitic rock the Bolmen tunnel in southwest Sweden infiltrating oxygenated rainwater dissolves ferrous iron minerals. The water becomes anoxic and dissolves ferrous iron minerals, but as it emerges into the air in the tunnel the ferrous iron is oxidized to ferric iron mediated by microbial activity, and the

iron precipitates as ferric hydroxide. This together with the microbes precipitates and is seen as the reddish streams. Detailed mapping was done in the Kymmen tunnel (Pamquist and Stanfors 1997). The channel density in the tunnel varied considerably, often there were only one or two channels in the more prominent, longer, fractures; most of the fractures did not have visible channels. Often flow was seen at fracture intersections.

In the 3D flow and tracer experiment at Stripa underground research laboratory, URL (Abelin et al. 1991) the 9 tracers injected in 9 different points, 11 to 50 m above the drift, were found in different locations and in different proportions in the 175 collection locations, sometimes bypassing paths taken by other tracers in the 3D network of channels. This showed that a complex channel network was present on the scale $70 \times 50 \times 5$ meters. Similarly in the smaller scale channelling experiment over some meter distances in a "prominent" fracture with a special "multipede" packer, also at Stripa, a complex channel network was found to exist as the injected tracers also arrived in 5 different locations on the face of the drift outside the "prominent" fracture. This was in addition to flowpaths in the "prominent" fracture in which the experiment was aimed to have most of the flow (Abelin et al. 1994). This was similar to the earlier findings in the 3D experiment but on a smaller scale. Unexpected flowpaths in the rock outside the "prominent" fracture were found in a third experiment, the 2D experiment (Abelin et al. 1983) and the TRUE experiment at Äspö URL (Neretnieks and Moreno 2003).

Numerical experiments with fractures with variable aperture have shown channelling effects with one or a few paths that carry most of the water (Tsang and Tsang 1987, 1989, Tsang et al. 1988, Moreno et al. 1988). It is found that even small shearing of fractures induces channelling (Min et al. 2004, Auradou et al. 2006, Koyama et al. 2009). This further supports the above observations.

Consequences of channelling are the main theme of this paper and we discuss its impact on solute transport especially considering radial diffusion from the channel into the rock matrix. Diffusion in the porous rock matrix causes retardation of solutes carried by the flowing water in fractured rock (Neretnieks 1980, Neuman 2005, Crawford 2008). Channels are assumed to be flat features and any diffusion in and out of the matrix is assumed to be linear and perpendicular to the channel surface in practically all previous modelling (Neretnieks 1980, Sudicky and Frind 1982, Cvetkovic et al. 1999, 2004). It may be argued that this still captures the solute retardation correctly because even if the "fully open" fractures were divided into a number of ribbons and these were arranged in a 3D channel network the flowing water would be in contact with the same magnitude of flow wetted surface area, FWS, over which the solutes migrate in and out of the rock matrix. Similar results should be expected as was also found by Selroos et al. (2002).

Figure 1-1. *Water emerging from channels in the fractures is stained red by precipitating ferric hydroxide.*

However, when the channels are narrow, there will be a large number of channels that supply the same FWS per volume of rock as the sparse fully open fractures do. The channels in the network will be closer to each other than two fully open fractures in the DFN. Furthermore, and a central theme of this paper, when a channel is narrow it may be more realistic to model the matrix diffusion as if it were radial from a tube with the same FWS. This would be more realistic when the penetration depth of the diffusing solute grows larger than the channel width. Matrix diffusion geometry and radial diffusion from veins in soils, has been discussed by Molz (1981), Gerke and van Genuchten (1997) and by Carrera et al. (1998).

Radial diffusion has been shown to be much more effective than linear diffusion from a single channel with the same FWS as a flat channels (Rasmuson and Neretnieks 1986). It has not been previously studied how this affects the solute transport through a networks of channels.

Radial diffusion from a dense network of narrow channels also leads to that the rock between two nearby channels may be more rapidly accessed by the solute than the rock mass between large distant "fully open" fractures. In the extreme with a very dense channel network the entire water in the porous matrix will be rapidly accessible to the solute and the transport behaves as if the pores of the rock contributed to the flow porosity. The porosity of the network of flowing fractures is much smaller than that of the matrix in crystalline rocks such as granite and the solute would move proportionally slower. This applies already for non-sorbing solutes. Sorbing solutes will more rapidly have access to more sorption sites in the rock matrix and will be even more retarded than non-sorbing solutes.

One of the aims of this paper is to show that channels in fractures can lead to major differences for solute transport compared to discrete fracture models in which it is assumed that fractures are either closed or transmissive over their entire extent. Another aim is to demonstrate that solute transport by diffusion from narrow channels into the rock matrix can more effectively retard solutes. A third aim is to devise solution(s) to the flow and transport equations for flow in channel with radial exchange of solute with the rock matrix for use in channel network models. For this we need to have a way of describing how channels connect to each other and how close to each other the channels in the network are located in order to assess how the solute diffusion from one channel may interact with that from a neighbouring channel.

We have earlier used a channel network model, CNM, with linear matrix diffusion (Moreno and Neretnieks 1993, Gylling 1997, Gylling et al. 1999). In that model the channel intensity and transmissivity distribution from observations in boreholes and a measure of channel widths is needed. For visualization purposes the channels are arranged in a cubic lattice with the channels along the edges of the cubes. It is also assumed that fracture intersections can be transmissive, forming a channel, so that in each corner of the network up to six channels may intersect. The intensity of channels and their transmissivities are assigned from a population obtained from down-hole measurements such that when the network is subjected to a hydraulic change, stochastically the observed channel intensity and flowrates in the channel intersections in boreholes are reproduced. Should there be trends of preferential directions of fracture family orientations, as observed in the boreholes, the cubic grid can be "deformed" to account for this. If there is information of correlation between channel lengths and transmissivities this can be included when assigning transmissivities to nearby channels. Making the grid denser there readily incorporates channelling in fracture zones, where such exist.

In the following section a model for solute transport in a channel with radial diffusion in the rock of a solute is presented and its solution in Laplace space is given. It is shown how solute transport through flowpaths that traverse an arbitrary number of channels each with different properties can be modelled. The section following shows how the effluent concentration from a flowpath over time is obtained from the analytical solution in Laplace space by numerical inversion to time space. The section thereafter shows how mean channel length and channel density in the channel network is obtained from borehole hydraulic data and channel width. Examples of data from different sites are shown. A number of examples are presented for three nuclides with different properties. Finally we discuss the results and make some conclusions.

2 Modelling solute transport in channels

2.1 Solute transport in a circular channel

Figure 2-1 illustrates the propagation of a diffusing solute from a flat channel and from a circular channel with the same flow wetted surface. The flowrate and velocity are set the same in the flat and the circular channel. Therefore the circular channel must be thought of as being made up of a concentric slit. It is seen that radial diffusion will involve a larger volume of rock compared to linear diffusion. When solute from two parallel channels would start to interfere with each other, which is on the order of halfway between the two parallel channels, an impenetrable boundary is assumed to exist at radius r_y.

The following equations describe the two main mechanisms, advective flow in the x-direction and transport of solute with concentration c in the channel from which radial diffusion with pore diffusion coefficient D_p takes place, Concentration is denoted by c_p in the porewater of the rock matrix, which has porosity ε_p. Diffusion is only in the r-direction from the channel into the surrounding porous rock. The cylindrical channel has inner diameter r_i, which has the same FWS as the flat channel $r_i = W_f/\pi$. The volume of the flowing channel however is kept the same as that of the flat channel. At radius r_y solute will not pass.

For the nuclide, with pore water concentration c_p and decay constant λ

$$\frac{\partial c_p}{\partial t} = \frac{D_a}{r}\frac{\partial}{\partial r}\left(r\frac{\partial c_p}{\partial r}\right) - \lambda c_p \tag{2-1}$$

$D_a = \frac{D_p}{R}$ is the apparent diffusion, R is the retardation factor due to linear reversible sorption, $R = 1 + \frac{K_d \rho (1-\varepsilon_p)}{\varepsilon_p}$, K_d is the mass sorption coefficient, ρ the rock mineral density. The initial and boundary conditions for (2-1) are

$$c_p\left(t = 0, r_i < r < r_y, x\right) = 0 \tag{2-2}$$

$$c_p(t, r = r_i, x = 0) = c(t, x = 0) \tag{2-3}$$

$$\frac{\partial c_p(t, r=r_y, x)}{\partial r} = 0 \tag{2-4}$$

Neglecting sorption on the channel surface, for the channel at any location x the concentration c varies as

$$\frac{\partial c}{\partial t} = -u\frac{\partial c}{\partial x} + \frac{1}{b} D_p \varepsilon_p \left.\frac{\partial c_p}{\partial r}\right|_{r=r_i} - \lambda c \tag{2-5}$$

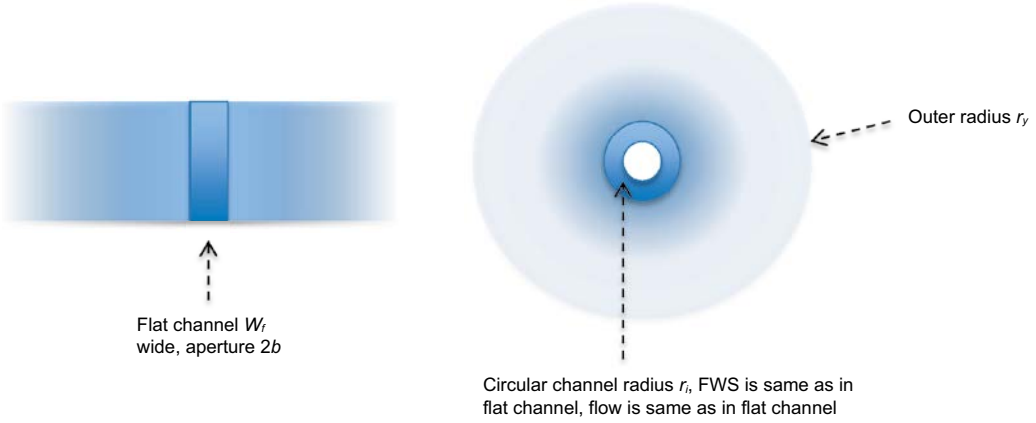

Figure 2-1. *Linear diffusion from a flat channel and radial diffusion from a circular channel.*

The term $1/b$ can be seen as the flow wetted surface of the channel to its volume $\frac{1}{b} = \frac{2\,W_f\,x_o}{2bW_f\,x_o}$ and this entity must be the same for the channel for both radial and linear diffusion because we need to maintain the same flow velocity and water residence time in the channel. Equation (2-5) is therefore valid for both cases. This implies, however, that the cylinder must be partly filled with a concentric solid smaller cylinder as shown in the right hand picture of Figure 2-1. Note that the fracture aperture b is very small compared to the width of the channel.

We intentionally do not include axial diffusion or dispersion. Diffusion could be readily incorporated in the model but it has a negligible effect, as does Taylor dispersion. Hydrodynamic dispersion is not a transport mechanism and its use in the advection dispersion model leads to strange effects that cannot readily be reconciled with observations and when modelling reactive solutes. See e.g. Neretnieks (2002a, b). It is often used to describe the spreading of a tracer pulse but in the opinion of this author it is not correct to model it as if it were equivalent to Fickian diffusion in fractured rocks because field experiments invariably show that the dispersion coefficient increases with measurement distance. However, as it is used in the advection dispersion equation it is taken to be constant when solving the equation. The dispersion coefficient, evaluated from tracer tests by curve fitting seems to increase in direct proportion to the scale of observations (Gelhar et al.1992, Gelhar 1993, Neuman 2005). The observed dispersion-path length dependence can be understood as being caused by differences in residence times in different flowpaths and not by a Fickian diffusion-like mechanism (Neretnieks 1983, 2002a, b, Chesnut 1994, Molz 2015).

The initial and boundary conditions are

$$c(t = 0, x) = 0 \tag{2-6}$$

$$c(t, 0) = c_{in}(t) \tag{2-7}$$

The system of equations will be solved using Laplace transformation. For the matrix the transformation gives

$$\widetilde{c_p}(s + \lambda) = \frac{D_a}{r}\frac{\partial}{\partial r}\left(r\frac{\partial \widetilde{c_p}}{\partial r}\right) \tag{2-8}$$

$$\widetilde{c_p}(x, r = r_i) = \widetilde{c}(x) \tag{2-9}$$

$$\frac{\partial \widetilde{c_p}(x, r = r_y)}{\partial r} = 0 \tag{2-10}$$

The solution to (2-8) to (2-10) is

$$\widetilde{c_p}(x, r) = \tilde{c}(x)\frac{J_1\left(\frac{ir_y\sqrt{s+\lambda}}{\sqrt{D_a}}\right) Y_0\left(-\frac{ir\sqrt{s+\lambda}}{\sqrt{D_a}}\right) + J_0\left(\frac{ir\sqrt{s+\lambda}}{\sqrt{D_a}}\right) Y_1\left(-\frac{ir_y\sqrt{s+\lambda}}{\sqrt{D_a}}\right)}{J_1\left(\frac{ir_y\sqrt{s+\lambda}}{\sqrt{D_a}}\right) Y_0\left(-\frac{ir_i\sqrt{s+\lambda}}{\sqrt{D_a}}\right) + J_0\left(\frac{ir_i\sqrt{s+\lambda}}{\sqrt{D_a}}\right) Y_1\left(-\frac{ir_y\sqrt{s+\lambda}}{\sqrt{D_a}}\right)} \tag{2-11}$$

J and Y are Bessel functions of first and second kind and $i = \sqrt{-1}$.

The gradient at the inner radius of the channels, which is needed to solve the equation for the channels is

$$\left.\frac{d\tilde{c}_p}{\partial r}\right|_{r=r_i} = \frac{\sqrt{s+\lambda}}{\sqrt{D_a}} B\tilde{c}(x) \tag{2-12}$$

$$B = i\frac{J_1\left(\frac{ir_y\sqrt{s+\lambda}}{\sqrt{D_a}}\right) Y_1\left(-\frac{ir_i\sqrt{s+\lambda}}{\sqrt{D_a}}\right) - J_1\left(\frac{ir_i\sqrt{s+\lambda}}{\sqrt{D_a}}\right) Y_1\left(-\frac{ir_y\sqrt{s+\lambda}}{\sqrt{D_a}}\right)}{J_1\left(\frac{ir_y\sqrt{s+\lambda}}{\sqrt{D_a}}\right) Y_0\left(-\frac{ir_i\sqrt{s+\lambda}}{\sqrt{D_a}}\right) + J_0\left(\frac{ir_i\sqrt{s+\lambda}}{\sqrt{D_a}}\right) Y_1\left(-\frac{ir_y\sqrt{s+\lambda}}{\sqrt{D_a}}\right)} \tag{2-13}$$

or the equivalent result with the modified Bessel functions I and K.

$$B = \frac{K_1\left(\frac{r_y\sqrt{s+\lambda}}{\sqrt{D_a}}\right) I_1\left(\frac{r_i\sqrt{s+\lambda}}{\sqrt{D_a}}\right) - K_1\left(\frac{r_i\sqrt{s+\lambda}}{\sqrt{D_a}}\right) I_1\left(\frac{r_y\sqrt{s+\lambda}}{\sqrt{D_a}}\right)}{K_1\left(\frac{r_y\sqrt{s+\lambda}}{\sqrt{D_a}}\right) I_0\left(\frac{r_i\sqrt{s+\lambda}}{\sqrt{D_a}}\right) + K_0\left(\frac{r_i\sqrt{s+\lambda}}{\sqrt{D_a}}\right) I_1\left(\frac{r_y\sqrt{s+\lambda}}{\sqrt{D_a}}\right)} \tag{2-14}$$

B only depends on the conditions in the matrix region.

Equation (2-5) with initial condition (2-6) by Laplace transformation gives at location x in the flowing channel

$$(s+\lambda)\,\tilde{c}(x) = -u\frac{d\tilde{c}(x)}{dx} + \frac{D_p\varepsilon_p}{b}\frac{d\tilde{c}_p}{\partial r}\Big|_{r=r_i} = -u\frac{d\tilde{c}(x)}{dx} + \frac{\varepsilon_p\sqrt{D_pR}}{b}\sqrt{s+\lambda}\,B\tilde{c}(x) \tag{2-15}$$

or

$$\left(s+\lambda - DG\sqrt{s+\lambda}\right)\tilde{c}(x) = -u\frac{d\tilde{c}(x)}{dx} \tag{2-16}$$

where

$$DG = \frac{\varepsilon_p\sqrt{D_pR}}{b}B \tag{2-17}$$

With boundary condition

$$\tilde{c}(x=0) = \tilde{c}_{in} \tag{2-18}$$

(2-16) and (2-18) have the solution

$$\tilde{c}(x) = \tilde{c}_{in}e^{-\frac{x(s+\lambda-DG\sqrt{s+\lambda})}{u}} \tag{2-19}$$

It is of some interest to study how different parameters and parameter groups will influence the results. The concentration is determined by the term $\frac{x\left(s+\lambda-DG\sqrt{s+\lambda}\right)}{u}$, which can be divided in two: $\frac{x(s+\lambda)}{u}$ and $\frac{xDG\sqrt{s+\lambda}}{u}$. The first term contains the water residence time $t_w = x/u$ in the path. The second term can be written

$$DG\frac{x}{u} = \frac{\varepsilon_p\sqrt{D_pR}}{b}\frac{x}{u}B = \varepsilon_p\sqrt{D_pR}\,\frac{x2W_f}{q}B = MPG \times \frac{A_q}{q} \times B \tag{2-20}$$

MPG is called the materials property group, which only contains entities that depend on the materials properties. The group $\frac{x2W_f}{q} = \frac{A_q}{q}$, which is the flow wetted surface A_q in the channel divided by the flowrate q in it. It is further noted that the half-fracture aperture b does not influence $DG\frac{x}{u}$, Equation (2-20). The aperture and thus water velocity u will influence the breakthrough curve by shifting the entire RTD by the water residence time $t_w = x/u$. This is a consequence of the first shift property of the Laplace transformation by the term $e^{-\frac{xs}{u}}$ in Equation (2-19). When matrix diffusion considerably retards the solute, the water residence time and the fracture aperture can be expected to have a minor or even negligible impact on the tracer break through curve, BTC. A_q/q will together with the MPG strongly impact the BTC. The entity *B* influences the results via the tube radius $r_i = \frac{W_f}{\pi}$, r_y and the apparent diffusivity $D_a = \frac{D_p}{R}$ in a complex manner, see Equation (2-13).

2.2 Transport in a flat channel

We want to compare the transport in the flat channels with linear diffusion with that when the diffusion is radial. The equations for the former are presented below. For a flat channel with linear diffusion (2-1) instead is

$$\frac{\partial c_p}{\partial t} = D_a\frac{\partial^2 c_p}{\partial z^2} - \lambda c_p \tag{2-21}$$

and the gradient at z = 0 is

$$\left.\frac{d\tilde{c}_p}{\partial z}\right|_{z=0} = \frac{\sqrt{s+\lambda}}{\sqrt{D_a}}\left(\frac{2}{1+e^{\frac{2\sqrt{s+\lambda}}{\sqrt{D_a}}z_y}} - 1\right)\tilde{c}(x) \tag{2-22}$$

z_y is the distance to the reflection boundary where the gradient is zero, analogous to Equation (2-10) for the radial diffusion case

For linear diffusion

$$B = \frac{2}{1+e^{\frac{2\sqrt{s+\lambda}}{\sqrt{D_a}}z_y}} - 1 \tag{2-23}$$

For very large distance between the channels $z_y \rightarrow \infty$, $B = -1$ whereas for radial channels B depends on $r_i\sqrt{\frac{s+\lambda}{D_p}}$ when $r_y \rightarrow \infty$.

2.3 Transport in a path consisting of a number of channels in series

A path consists of a number of channels that the solute passes. In a network of channels the effluent concentration from one channel contributes to the inlet concentration to another channel. One can determine the multitude of paths from one or more starting positions by e.g. particle tracking and keep track of the flowrates and other properties of each channel. With this information the effluent concentration from the last channel at the effluent location can be obtained in each path by convolution, which in Laplace space is done by a simple multiplication using (2-19) for each consecutive channel "j" in the path.

The effluent from channel "1" is

$$\tilde{c}(x_1) = \tilde{c}_{in}e^{-\frac{x_1}{u_1}(s+\lambda-DG_1\sqrt{s+\lambda})} \tag{2-24}$$

This contributes to the inlet concentration to channel "2", which then has an effluent concentration

$$\tilde{c}(x_2) = \tilde{c}_{in}e^{-\frac{x_1}{u_1}(s+\lambda-DG_1\sqrt{s+\lambda})}e^{-\frac{x_2}{u_2}(s+\lambda-DG_2\sqrt{s+\lambda})} \tag{2-25}$$

In the same way any number of channels in a path can be followed. The outlet from the last channel "N_k" in this path is

$$\tilde{c}_{N_k} = \tilde{c}_{in}\prod_{k=1}^{N_k}e^{-\frac{x_k}{u_k}(s+\lambda-DG_k\sqrt{s+\lambda})} = \tilde{c}_{in}e^{-\sum_{k=1}^{N_k}\frac{x_k}{u_k}(s+\lambda-DG_k\sqrt{s+\lambda})} \tag{2-26}$$

With $t_w = \frac{x}{u}$ and $DG = MPG\frac{A_q}{q}B$

$$\tilde{c}_{N_k} = \tilde{c}_{in}e^{-\sum_{k=1}^{N_k}t_{w,k}(s+\lambda)}e^{\sum_{k=1}^{N_k}MPG_k(\frac{A_q}{q})_kB_k\sqrt{s+\lambda}} \tag{2-27}$$

If, for example by particle tracking, in the channel network with known flowrates, widths, apertures and material properties in each channel the different paths (large number) consisting of the different "channels" is known the sum of residence times in each channel in the path adds up to the total residence t_j in path j. Similarly the total flow wetted surface to flowrate for the path times the materials property group could be obtained. Also B_k varies between channels and has to be determined for each channel.

The total concentration at an effluent point is obtained by sum of solute flowrates divided by sum of water flowrates from all paths ending in that effluent location.

3 Numerical inversion method

The solutions presented earlier are in Laplace space. They need to be inverted to time space. The equations are not readily inverted analytically and numeric methods must be used. With *F(s)* being the function in Laplace space to invert to *f(t), F(s)* in this case is given by Equation (2-27). The inverse Laplace transform is a complex inversion integral given by

$$f(t) = \frac{1}{2\pi i} \int_{\gamma-i\infty}^{\gamma+i\infty} e^{st} F(s) ds \tag{3-1}$$

The inversion is done numerically by Fourier function approximation of *F(s)*. We use a discretized form of the inversion integral (de Hoog et al. 1982, Boupha et al. 2004).

$$f(t) = \frac{e^{\sigma t}}{T}\left(\frac{1}{2}F(\sigma) + \sum_{k=1}^{\infty}(Re(F(\sigma + k\pi i T))\, e^{k\pi i t/T}\right. \tag{3-2}$$

Re(F(s)) denotes the real part of the complex-valued *F(s)*, where $\sigma = \sigma_o - \frac{Ln(Er)}{2T}$. The parameters *Er*, σ_o and *T* were chosen to be 10^{-8}, 0 and $2.5 \times t_{max}$ respectively, where t_{max} is the largest time in the time range of interest. These values were selected after a number of tests inverting functions with known analytical expressions for *F(s)* and *f(t)*. To accelerate the convergence of the infinite series summation we use the Method "WynnEpsilon" in the numeric summation routine "NSum" in Mathematica® (Wolfram Research Inc. 1988–2014). The largest errors were a few tenths of one percent but were mostly much smaller on the order of 10^{-5} c/c_o. Figure 3-1 shows the error in the example case shown in Figure 5-1, for linear diffusion using the analytical solution of Neretnieks (1980) for $z_y \rightarrow \infty$. The number of terms used before extrapolation was 1 000 in this example. For radial diffusion often much fewer terms mostly gave stable results. Similar errors were found for the two example cases used by de Hoog et al. (1982). An alternative would be the commonly used implementation of the de Hoog algorithm INVLAP in MATLAB (Hollenbeck 1998), which is considerably more sophisticated.

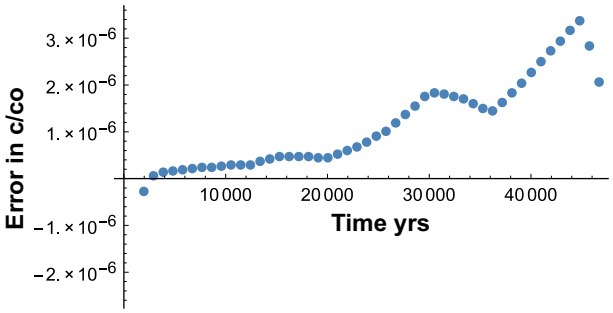

Figure 3-1. *Example of error between analytic and numerically inverted results for a case where c/co varies from 0 to 0.8.*

4 Channel Network Modelling

4.1 Obtaining data for a channel network model

The intensity of channels, their lengths, widths, transmissivities and apertures can be estimated from in-situ measurements and from other sources. One set of data is the number of intersections of water conductive fractures per meter borehole that traverses the rock mass of interest, $P10_{flow}$ (number of fractures per m). The specific flow wetted surface for solute interaction can be assessed from the intensity of water conductive fractures $P32_{flow}$ (m^2 fracture surface/m^3 rock), which is twice this number. $P32_{flow}$ is usually determined from $P10_{flow}$, modified by fracture orientations to account for the smaller chance of intersecting fractures that are not perpendicular to the borehole, using the Terzaghi correction.

Measurements of fracture/channel intensities $P10_{flow}$ can be made by shutting off short lengths of a borehole in the rock by packers and injecting/withdrawing water or by other flow techniques or meters e.g. the Posiva flow tool (Öhberg and Rouhiainen 2000). This gives information of the flowrate distribution in the flowing fractures. From this information the transmissivity distribution of the channels can be estimated.

A detailed discussion on fracture intensity measures can be found in Dershowitz et al. (1998). In the site investigation of the Laxemar site it was found that only 2.7 % of all 64 452 fractures observed in deep boreholes intersected conductive channels (Rhén et al. 2008). Detailed inspection of the drill cores showed that of all the borehole/fracture intersections 10.6 % were classified as being open. At Laxemar $P10_{flow} = 0.11\ m^{-1}$ which means that at repository depth in the boreholes one fracture with a conducting channels was found every 9 metres. It also showed that there were about 35 fractures that were not conducting for every conducting fracture, or rather that the closed parts of these fractures were intersected. At the Forsmark site, of 34 191 fractures totally 1.7 % were conductive and 7.1 % were classified as open or partly open (Follin 2008). If instead of assuming that fractures are either transmissive over their entire size or entirely non-conducting all fractures have channels the channels would on average make up a few percent of the entire fracture surface in the two sites mentioned.

Channel widths cannot be determined from borehole measurements. Observations are made in drifts and tunnels where the channel surface density, CSD, expressed as number of channels per m^2 and channels widths can be measured. Channel widths are often found to be a few mm to several tens of cm. In our CNM channel lengths are basically equal to the size of the cubes in the grid. If information is available on the persistence of extensive flowpaths this can be incorporated by assigning the same or similar properties to a number of directly connected channels.

4.2 Arrangement of channels in the network

For visualization purposes the channels are arranged in a cubic network. If the cube were made up of fractures that are transmissive everywhere with sizes $L_{large} \times L_{large}$, where L_{large} is the edge length of the cube surrounded by fully open fractures, the fracture intensity $P32_{flow}$ m^2/m^3 rock is

$$P32_{flow} = \frac{3}{L_{large}} \tag{4-1}$$

If the fully open fracture is divided in "strips = channels" with width W_f their total area in the rock mass must sum up to the same intensity $P32_{flow}$ as the value found with the fully open fraction assumption. These channels are placed at the edges of smaller cubes with an edge length of L_{small}. Each edge has area $W_f L_{small}$, which is shared by four cubes. $P32_{flow}$ is the same for both small and large cubes, which gives

$$L_{small} = \sqrt{W_f L_{large}} \tag{4-2}$$

Another way of estimating the channel width is from observations of channel surface density seen on the walls of drifts and tunnels. In the cubic grid CSD is approximately equal to L_{small}^{-2}. Then

$$W_f = \frac{P32_{flow}}{3CSD} \tag{4-3}$$

Direct observations of channels widths range from mm to some tens of cm (Abelin et al. 1983, 1985, 1994). See also Tsang and Neretnieks (1998) for an overview of channelling experiments and observations on different scales. Some observations of channel data are given in Table 4-1. These data have been gathered in rock that lies outside of larger fracture zones. In fracture zones the fracture frequency is considerably larger as is also the transmissivity of the channels. The Stripa 3D and SFR information has been used to simulate and analyse the frequency of flowrates and channel density distributions for use in the channel network model (Moreno and Neretnieks 1991). That report also discusses how channel widths can be assessed. The observation times in those experiments are short and only small impact of radial diffusion is expected to be seen. Radial diffusion will start to influence solute transport after tens to thousands of years in the type of fractured crystalline rocks discussed here.

The number of possible paths through the network is immense even for rather small networks. However it is not necessary to know all possible paths that can be taken by a particle entering the channels network to obtain acceptably good simulations of solute transport through the network by stochastically generating a number of paths by particle tracking based on the probability density functions of the parameters. The idea is similar to Monte-Carlo integration. In *fracture* network modelling less than 10 000 paths were deemed to give sufficiently reliable results for the purpose of performance assessment (Joyce et al. 2010).

Table 4-1. Observations of channelling and other data on channels in rock between large fracture zones.

Location and/or experiment	Channel width W_f m	Channel surface density CSD m^{-2} (m^2/channel)	Fracture intensity $P32_{flow}$ m^{-1}	Conductivity of fracture network K m s^{-1}	Comments	Reference
Stripa 2D	0.1–0.2	NA	NA	NA	Single fracture 5 m, at 360 m depth	Abelin et al. (1983, 1985)
Stripa 3D	0.034–0.34 from 5 tracer retardation data	0.145 (6.9)	0.1–14 from 5 tracer retardation data	$(0.6–3.6) \times 10^{-11}$	Observation area 750 m^2, at 360 m depth, flow porosity $2–16 \times 10^{-5}$	Abelin et al. (1991)
Stripa Channelling	0.001–0.1	NA	NA	NA	Along a 1.95 m long fracture	Abelin et al. (1994)
Kymmen	0.01–0.3	0.0095, (105)	NA	NA	In tunnel over several km	Neretnieks (1984), Palmquist and Stanfors (1987)
Bolmen	0.01–0.3	Around 0.01–0.02, (50–100)	NA	NA	In tunnel over several km	Stanfors (1987)
SFR	0.01–0.3	0.029, (35) over 14 000 m^2,	NA	$(1.5–6.8) \times 10^{-7}$	At repository depth > 100m	Neretnieks (1984), Holmén and Stigsson (2001)
Äspö, True 1 experiment	NA	NA	4.5	1×10^{-8}	Tracer experiments at 400 m depth over 5–10 m distance	Neretnieks and Moreno (2003)
Laxemar	NA	NA	0.08–0.55	$(0.4–20)\times 10^{-8}$	At around 150–400 m depth	Rhén et al. (2008)
Laxemar	NA	NA	0.06–0.26	$(0.2–3) \times 10^{-8}$	400–650 m	–"–
Laxemar	NA	NA	0.005–0.023	$(0.1–7) \times 10^{-8}$	< 650 m	–"–
Forsmark	NA	NA	0.09–0.33	1×10^{-7}	0–200 m depth	Follin (2008), Hartley and Roberts (2013), Joyce et al. (2010)
Forsmark	NA	NA	0.07	3×10^{-10}	200–400 m depth	–"–
Forsmark	NA	NA	0.005	4×10^{-11}	> 400 m	–"–
Other	0.1– 0.3	–	NA	NA	On outcrops, Neretnieks personal obs.	

A case of special interest is when the source term is subject to radioactive decay. For a decaying band release, $c_{in} = c_o e^{-\lambda t}$, the Laplace transformed $\tilde{c}_{in} = \frac{c_o}{s+\lambda}$ This is used in the examples. The hydraulic conductivity K in the table is taken from data on mean transmissivities over a depth interval in the boreholes and from of equivalent continuous porous medium, ECPM, calculations using DFN models. The former agree fairly well with ECPM estimates on 100 m cubes. The K-values can vary considerably between boreholes and between realizations in ECPM.

For only one of the sites in Table 4-1 there is information on fracture widths, flowing fracture intensity as well as channel surface density. This is from the 3D experiment in the underground research laboratory at Stripa (Abelin et al. 1991). The experiment is unique in that tracer arrival was studied in a large number of locations on the walls of the drift where the 11 different tracers from nine different injection locations, 11 to 50 m above the drift were collected. In this 3D flow and tracer migration experiment a drift 100 long in fractured granite at 360 m depth, was excavated for the experiment. It was covered with 375, 2 m^2 size plastic sheets on walls and ceiling to collect water and tracers over more than 2 years. The rock is fully saturated deeper than a few meters below ground surface. The flowrate, which was constant throughout the experiment and tracer concentration evolution over time in each sheet, gave information on residence time distributions from different flowpaths. 160 different tracer breakthrough curves, covering a period of 2 years were analysed. Many of them had more than one peak. It was possible to estimate channel widths, flow porosities and how the tracers interacted with stagnant water in the rock matrix and in the fractures themselves. Estimates of flowing channel frequencies were also made.

All this information is not available in any one of the other sites. The channel width seems to be the only entity that is found to be in the same range for all sites. For only one of sites, Stripa 3D, there is information on flow porosity. As will be seen in the examples presented later the flow porosity is needed to determine the water residence time. However, it will also be shown that for performance assessment purposes this does not have an important influence for the long flowpaths and times of interest.

5 Examples

Some examples are used to illustrate the results and as a basis for discussion of the impact of different parameters. The data are chosen based on the detailed field and laboratory investigations of a large crystalline rock mass at Forsmark, which is the designated site for the Swedish repository for high level nuclear waste (SKB 2011). See Table 4-1 for details. The data in Table 5-1 have been selected as reasonably representative of the set of data available used in the modelling of flow and radionuclide transport from a repository at around 500 m depth. In the examples the distance from the repository vertically upward to the biosphere is chosen although most streamlines have a downward component, before turning upward. Joyce et al. (2010) using a fracture network model present stochastic simulation results on flowrates and transport related distributions for a repository at Forsmark. The values of the most important entity, A_q/q, in the examples presented below are well within those distributions.

In the examples only one path is used. It can be though of as one path found by particle tracking through the channel network. The numerical values for the entities in Equation (2-27) would represent a path where all the channels happen to have the mean values of the entities concerned. It is out of the scope of this paper to make a multitude of syochasic simulations of different paths.

Table 5-1. Parameter values used in the examples. Mainly taken from Hartley and Roberts (2013), Joyce at al. (2010), and Crawford (2008).

Notation	Value	Unit	Meaning
$\frac{A_q}{q} = \frac{2P32_{flow}x_o}{u_o}$	2.2×10^5 L 2.2×10^6 L 1.6×10^5 F 1.6×10^6 F	years/m	Flow wetted surface to flowrate, derived values. (L =Laxemar, F = Forsmark)
D_p	3×10^{-11}	m^2/s	Pore diffusion coefficient
grad	1×10^{-3}	m/m	Hydraulic gradient vertically upward
K	1×10^{-8} L 1×10^{-9} L, F 1×10^{-10} F	m/s	Mean hydraulic conductivity of rock mass
$P32_{flow}$	0.07 L 0.005 F	m^{-1}	Fracture intensity at Forsmark depth 150 to 400 m and deeper than 400 m
$T_{1/2}$	5730 1.57×10^7 2.3×10^6	years	^{14}C, Halflife ^{129}I ^{135}Cs
$u = u_o/\varepsilon_{flow}$	3.3×10^{-8} L 3.3×10^{-7} L, F	m/s	Water velocity in channels, derived values
$u_o = K \times grad$	10^{-13} F 10^{-12} L,F 10^{-11} L	$m^3/m^2/s$	Water flux upward in rock, derived values
W_f	0.03, 0.1, 0.3	m	Channel width
x_o	500	m	Travel distance from repository at 500 m depth to the ground surface
ε_p	3×10^{-3}	–	Rock matrix porosity
ε_{flow}	3×10^{-5}, L 3×10^{-6} F, L	–	Rock porosity of flowing fractures

The first example is for the very long-lived ^{129}I with $P32_{flow} = 0.07$. The breakthrough curves are shown in Figure 5-1 for linear diffusion as well as radial diffusion from the channel.

This example could illustrate transport in Forsmark rock with properties at depths between 200 and 400 m and Laxemar rock at repository depth around 500 m if the entire transport path was in this type of rock. The, would be, plug flow residence time of all fracture and pore water is 48 000 years. The residence time of the flowing water is 480 years (48 years for $\varepsilon_{flow} = 3 \times 10^{-6}$). It is seen that iodine emerges as if had been in equilibrium with a large fraction of all the pore water in the entire matrix when the diffusion is radial. Linear diffusion gives early breakthrough at around 500 years,

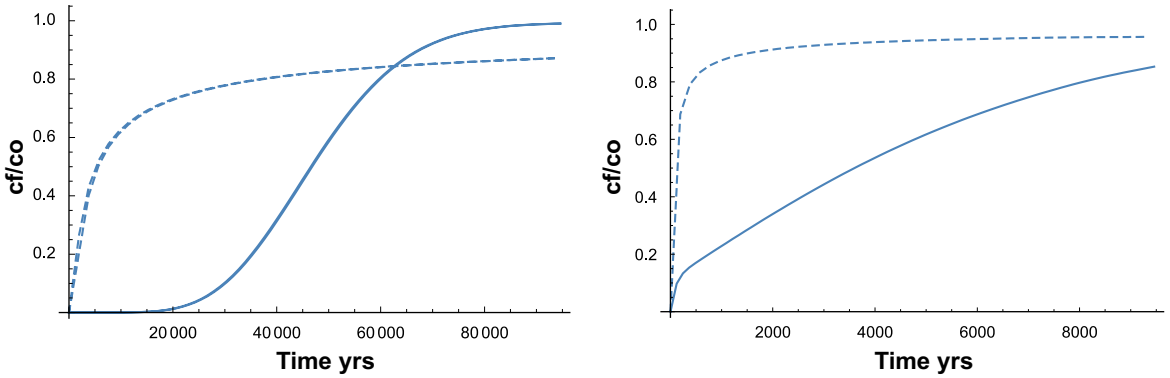

Figure 5-1. *^{129}I concentration at x = 500 m, $P32_{flow} = 0.07\ m^{-1}$, $W_f = 0.1$ m, $\varepsilon_{flow} = 3 \times 10^{-5}$ as well as $\varepsilon_{flow} = 3 \times 10^{-6}$ (Indistinguishable curves). Cylindrical diffusion full line and dashed line for linear diffusion. Left figure $K = 10^{-9}$, right figure $K = 10^{-8}$ m/s. Note the different time scales in the figures.*

the residence time for the flowing water. With a 10 times smaller flow porosity the results are practically not distinguishable in the graph. This is expected and fortunate because flow porosities and fracture apertures are difficult to assess. For this case $L_{large} = 43$ m and $L_{small} = 2.9$ m . This implies the outer radius r_y of the cylinder is 1.45 m and the channel is 2.9 m long. The pore water in the rock in this cylinder will be nearly equilibrated after about 80 000 years. For the fracture network the 43 m distance between fractures only permits a small fraction of the rock to equilibrate and the BTC comes earlier.

Figure 5-2 shows the results for the extremely small value of $P32_{flow} = 0.005\ m^{-1}$. It represents the unusually tight rock at repository depth at Forsmark chosen to host the Swedish high-level nuclear waste repository (SKB 2011). This rock has very few conducting fractures. The spacing between the "fully flowing" fractures, if they were arranged on a cubic grid is 600 m in the CNM. The channel length would be about 8 m. Also here the non-sorbing species is considerably delayed compared to the linear diffusion case. In Figure 5-1 the FWS is 14 times larger. On the other hand the conductivity and so the flowrate is 10 times lower in Figure 5-2 than in Figure 5-1. The FWS to flowrate ratio A_q/q only differs by a factor 1.4 but the results are very different. Note the different time scales in Figures 5-1 and 5-2.

This highlights the other aspect of the difference between channel network and fracture network properties. It is not only the fact that radial diffusion in a channel network gives larger retardation than linear diffusion for a given A_q/q, but that a narrow channel width implies that the channels must lie closer to each other to accommodate the same FWS per rock volume. It is the latter effect that gives the very large difference in BTC's between Figure 5-1 and Figure 5-2.

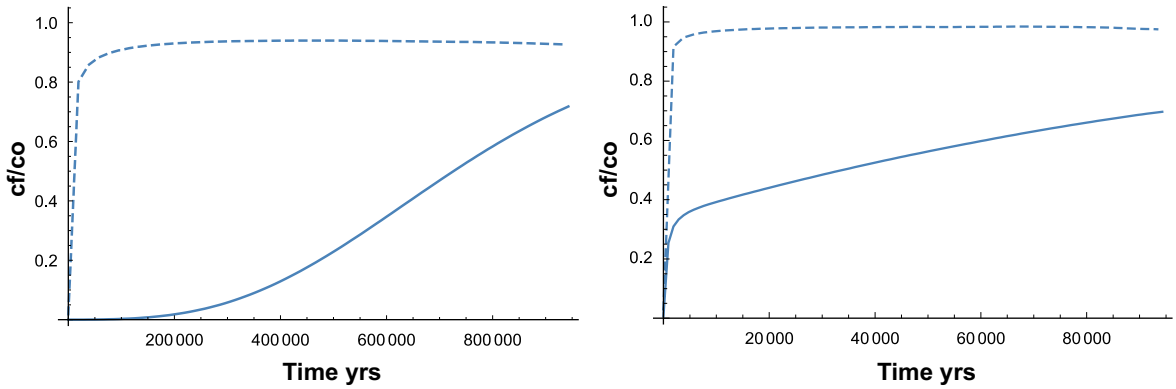

Figure 5-2. *^{129}I concentration at x = 500 m, $P32_{flow} = 0.005\ m^{-1}$, $W_f = 0.1$ m, $\varepsilon_{flow} = 3 \times 10^{-6}$ Cylindrical diffusion full line and dashed line for linear diffusion. Left figure $K = 10^{-10}$, right figure $K = 10^{-9}$ m/s.*

Figure 5-3 shows that the difference between the cylindrical and flat channels increases strongly with decreasing fracture intensity P_{32}.

Figure 5-4 shows the results for a 0.3 m wide channel with the same data as in Figure 5-1. The difference is not very large

Below an example is given for also a non-sorbing ^{14}C compound such as $^{14}CO_3^{2-}$ or $^{14}CH_4$. The half-life of ^{14}C is 5 730 years, which is much shorter than ^{129}I and can be expected to partly decay during its passage. Figure 5-5 shows results with the same data as those in Figure 5-1. The figure is divided in two sub-figures because the concentrations are very different. It is seen that ^{14}C decays by several orders of magnitude more in the cylindrical diffusion case.

Also sorbing tracers may be more delayed by the radial diffusion than by linear diffusion. This is illustrated in Figure 5-6 by ^{135}Cs with a half-life of 2.3×10^6 years and a retardation coefficient $R = 170$ in marine water (Crawford 2008). With radial diffusion the decay is 8 orders of magnitude larger compared to linear diffusion.

Figure 5-7 shows that at short travel distances radial and linear diffusion give the same results, as expected, and also shows that the Laplace solution agrees with the analytical solution at early times. The full line is obtained by the analytical solution with $z_y = r_y \rightarrow \infty$, which is valid for short times as well as with the Laplace transformed solution.

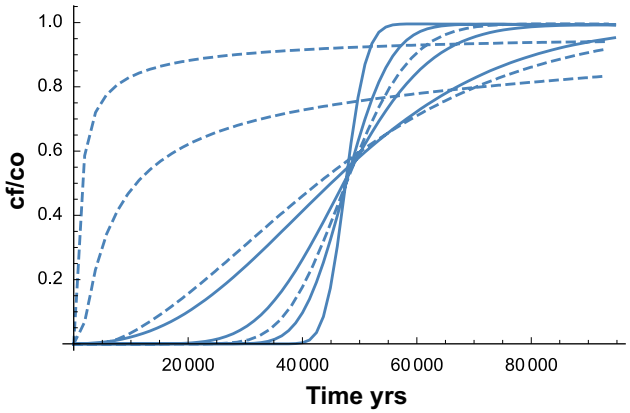

Figure 5-3. *^{129}I concentration at $x = 500$ m, $W_f = 0.1$ m, $K = 10^{-9}$ m/s. Cylindrical diffusion full line and dashed line for linear diffusion. $P32_{flow} = 0.03, 0.1, 0.3, 1$ m^{-1} from left to right.*

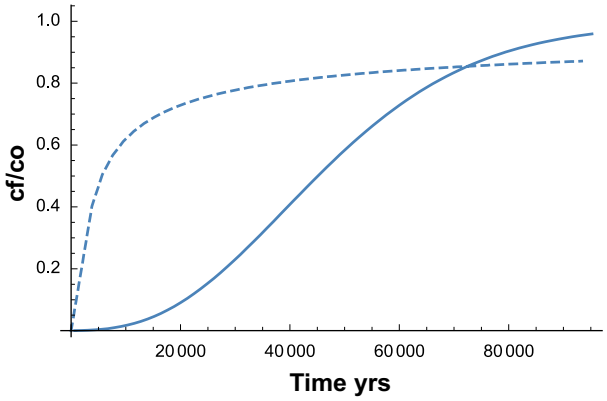

Figure 5-4. *^{129}I concentration at $x = 500$ m, for $P32_{flow} = 0.07$ m^{-1} and $W_f = 0.3$m, $K = 10^{-9}$ m/s. Cylindrical diffusion full line and dashed line for linear diffusion.*

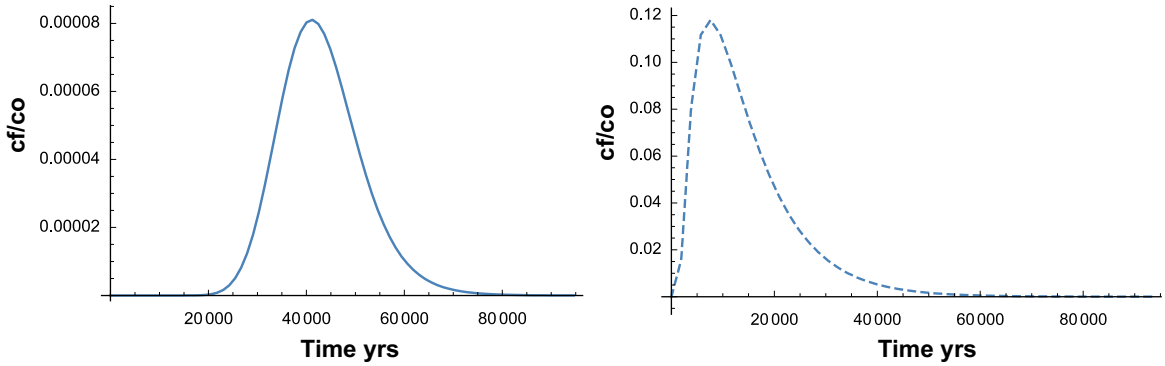

Figure 5-5. *^{14}C concentration at x = 500 m, for $P32_{flow} = 0.07\ m^{-1}$ and $W_f = 0.1$ m, $K = 10^{-9}$ m/s. Cylindrical diffusion, left figure and linear diffusion, right figure.*

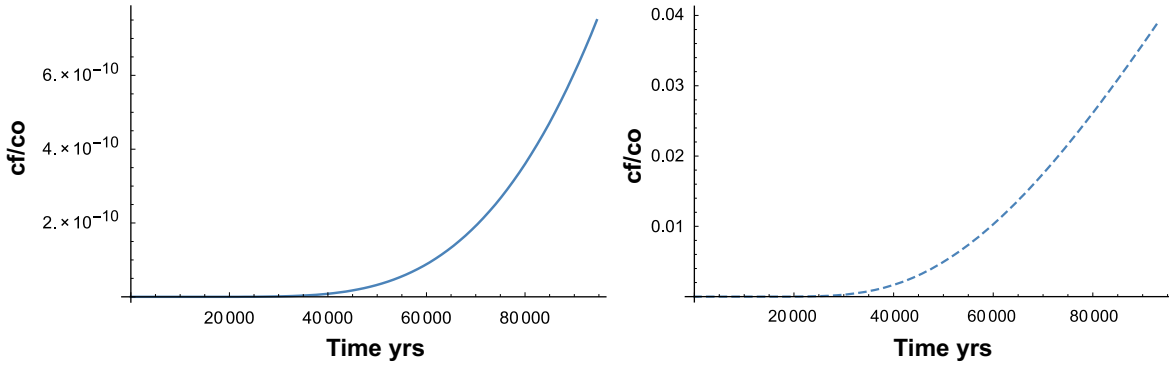

Figure 5-6. *^{135}Cs concentration at x = 500 m, for $P32_{flow} = 0.07\ m^{-1}$ and $W_f = 0.1$ m, $K = 10^{-9}$ m/s. Cylindrical diffusion, left figure and linear, right figure.*

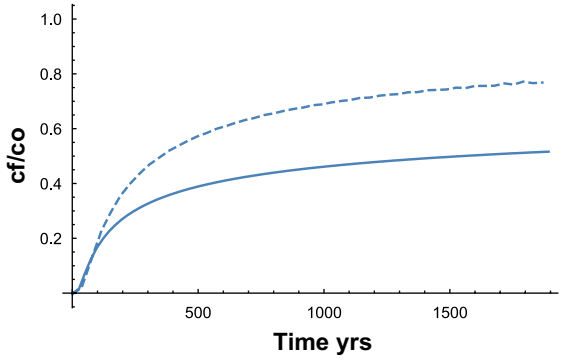

Figure 5-7. *^{135}Cs concentration at x = 10 m, for $P32_{flow} = 0.07\ m^{-1}$ and $W_f = 0.1$ m, $K = 10^{-9}$ m/s. Cylindrical diffusion full line and dashed line for linear diffusion.*

Figure 5-8 shows the impact of channel width for ^{135}Cs. With a width of 0.3 m instead of 0.1 m as in Figure 5-6 the concentration has increased by 5 orders of magnitude. On the other hand a 0.03 m channel retards ^{35}Cs by an additional 14 orders of magnitude.

The dramatic impact on the retardation by the channel width can be understood by analysing how much of the matrix is accessed when the channel density increases with decreasing channel width. Table 5-2 shows the size of the cubes along which the channels are aligned. The radius at which the concentration is 0.5 c_o and the fraction of rock in the region up to r_y that has been equilibrated to c_o after 100 000 years are shown. These entities can be obtained directly from the solution of radial concentration profile. It is seen that smaller channels give rise to higher density of channels, which in turn leads to a larger fraction of the rock to participate in the retardation.

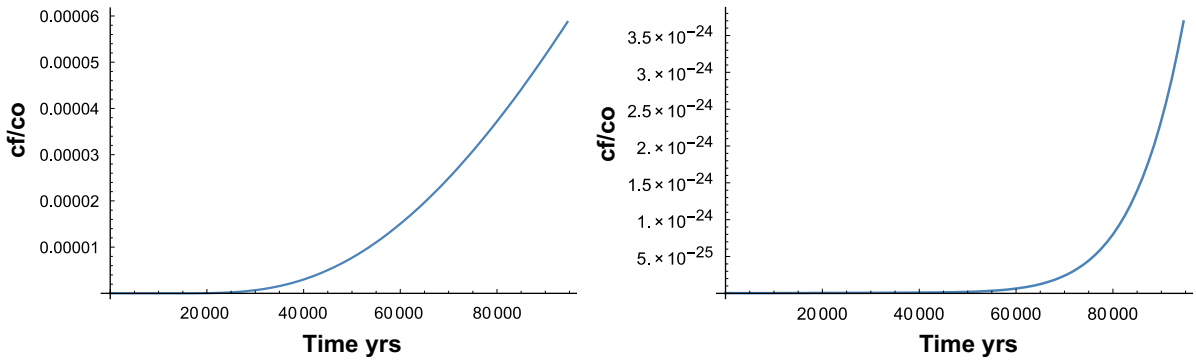

Figure 5-8. *^{135}Cs concentration at x = 500 m, for $P32_{flow} = 0.07\ m^{-1}$ and $W_f = 0.3$ m, $K = 10^{-9}$ m/s, left figure and 0.03 m right figure.*

Table 5-2. Example of impact of channel widths on retardation of a sorbing nuclide, ^{135}Cs.

W_f, m	L_{small}, m	Penetration radius of 0.5 c_o at inlet of tube, m	Fraction of rock equilibrated to c_o at inlet of tube
0.03	1.6	0.18	0.21
0.1	2.9	0.22	0.076
0.3	5.1	0.28	0.030

6 Discussion and conclusions

Selroos et al. (2002) compared the properties of different model concepts. In the examples used they found that the discrete fracture network model, the channel network models and also the stochastic continuum model predict similar behaviour of solute fluxes and travel times. However, in all these models including the channel network model they modelled the diffusion as one-dimensional and orthogonal to the flat fracture/channel surface. Then it is expected that the models give similar results because the results essentially depend on the ratio of the flow-wetted surface to the flowrate A_q/q in the pathways, which were essentially the same.

In this report we use an alternative mode of diffusion because of the presence of channels in the fractures and of the way the networks are conceptualized. In discrete fracture network models used to simulate flow and transport of solutes that diffuse in and out of the rock matrix it is assumed that the diffusion takes place orthogonally to the fracture surface. The transmissive fractures are modelled as being transmissive over their entire area. These assumptions lead to a sparse network of conducting, "fully open" fractures in a rock with a much larger number of "fully closed" fractures. Besides that "fully open" fractures are not physically realistic and that such a network may be poorly connected it also implies that solutes diffusing in the rock matrix may reach only a small fraction of the rock matrix during the time of interest. If in contrast to the fully open or fully closed fracture assumption flow takes place in a multitude of channels that may exist in a large portion of, or even all, fractures the distance between channels will be much smaller than the distance between the "open" fractures.

From narrow channels the diffusion will become increasingly more radial as the diffusion penetration depth increases. This leads on the one hand to a larger solute flux from the flowing channel and on the other hand to a more rapid equilibration of the rock between the channels because the radial ingress of the solute contacts more rock. These effects lead to a considerably, even very much, larger retardation of the solutes.

Our most important assumptions are that channels are narrow and that they contribute as large a flow wetted surface as the "open" fractures in the DFN model do. This ensures that the flow-wetted surface is the same in both model concepts. Note that the FWS is obtained from field measurements and does not depend on if a channel network or a fracture network will be modelled. Field observations of channel widths and of channel surface densities as seen on rock faces and flowing fracture intensities as seen in boreholes, although from different sites and experiments, support the concept of channel networks in preference to fracture network with fully open/closed fractures. Numerous modelling papers on channels flow in individual fractures also strongly support the channelling concept.

A_q/q is used as a performance measure and is called Flow-related transport resistance F_r in Joyce et al. (2010). It is one of the most important entities that influence the nuclide transport. The larger it is the stronger will be the retardation of the nuclides. In the examples given in this paper the values are on the low end of those presented in Joyce et al. (2010) who use a stochastic fracture network model with linear diffusion. Less than 3 % of all paths have A_q/q lower than 2×10^5 yr/m and less than 25 % have less than 2×10^6 yr/m, which are the values in the present examples, see Table 5-1. This implies that if the same distribution of A_q/q paths were found with the CNM the retardation would be considerably larger for the vast majority of the flowpaths.

There are several challenges that must be addressed in order to be able to use channel network models with confidence to predict solute transport in large rock masses. Channel widths cannot be determined from borehole measurement techniques; underground observations are needed. Similarly independent information on channel surface density can at present only be determined by observations on rock faces, which only can be done underground at the actual site. Another challenge is to assess persistency of flowpaths, i.e. how long a flowpath may be with essentially the same (large) flowrate. If there exist long preferential flowpaths, e.g. in large fractures, without considerable breaking up into smaller channels and re-joining with other channels, channelling may lead to fast paths with little retardation (Oden et al. 2008). This problem is, however common with all other models.

The findings that ^{129}I and ^{14}C are much more retarded in channel network than in fracture network simulation can have consequences for safety assessments for high level waste repositories in crystalline rocks, especially during the first 10 000 years, should canisters fail early. These two nuclides often give a considerable contribution to the dose calculations in hypothetical "what-if cases" with early release (SKB 2011, Section 13.7).

References

SKB's (Svensk Kärnbränslehantering AB) publications can be found at www.skb.com/publications.

Abelin H, Gidlund J, Moreno L, Neretnieks I, 1983. Migration in a single fissure in granitic rock. In McVay G L (ed). Scientific basis for nuclear waste management VII: symposium held in Boston, Massachusetts, 14–17 November 1983. New York: North-Holland. (Materials Research Society Symposium Proceedings 26), 239–246.

Abelin H, Neretnieks I, Tunbrant S, Moreno L, 1985. Final report on the migration in a single fracture. Experimental results and evaluation. Stripa Project Technical Report 85-03, Svensk Kärnbränslehantering AB.

Abelin H, Birgersson L, Moreno L, Widén H, Ågren T, Neretnieks I, 1991. A large-scale flow and tracer experiment in granite II. Results and interpretation. Water Resources Research 27, 3119–3135.

Abelin H, Birgersson L, Widén H, Ågren T, Moreno L, Neretnieks I, 1994. Channeling experiments in crystalline fractured rocks. Journal of Contaminant Hydrology 15, 129–158.

Amadei B, Illangasekare T, 1994. A mathematical model for flow and transport in non-homogeneous rock fractures. International Journal of Rock Mechanics and Mining Sciences & Geomechanics Abstracts 31, 719–731.

Auradou H, Drazer G, Boshan A, Hulin J-P, Koplik J, 2006. Flow channeling in a single fracture induced by shear displacement. Geothermics 35, 576–588.

Berkowitz B, 2002. Characterizing flow and transport in fractured geological media: a review. Advances in Water Resources 25, 861–884.

Birgersson L, Widén H, Ågren T, Neretnieks I, 1992. Tracer migration experiments in the Stripa mine 1980–1991. Stripa Project Technical Report 92-25, Svensk Kärnbränslehantering AB.

Birgersson L, Moreno L, Neretnieks I, Widén H, Ågren T, 1993. A tracer migration experiment in a small fracture zone in granite. Water Resources Research 29, 3867–3878.

Bodin J, Delay F, de Marsily G, 2003a. Solute transport in a single fracture with negligible matrix permeability: 1. fundamental mechanisms. Hydrogeology Journal 11, 418–433.

Bodin L, Delay F, de Marsily G, 2003b. Solute transport in a single fracture with negligible matrix permeability: 2 mathematical formalism. Hydrogeology Journal 11, 434–454.

Boupha K, Jacobs J M, Hatfield K, 2004. MDL Groundwater software: Laplace transforms and the De Hoog algorithm to solve contaminant transport equations. Computers & Geosciences 30, 445–453.

Brown S, Caprihan R, Hardy R, 1998. Experimental observations of fluid flow channels in a single fracture. Journal of Geophysical Research 103, 5125–5132.

Cacas M C, Ledoux E, de Marsily G, Tillie B, A Barbreau, E Durand, Fuega B, Peaudecerf P, 1990a. Modeling fracture flow with a stochastic fracture network: Calibration and validation: 1. The flow model. Water Resources Research 26, 479–489.

Cacas M C, Ledoux E, de Marsily G, Barbreau A, Calmels P, Gaillard B, Margitta R, 1990b. Modeling fracture flow with a stochastic fracture network: Calibration and validation: 2. The transport model. Water Resources Research 26, 491–500.

Carrera J, Sánchez-Vila X, Benet I, Medina A, Galarza G, Guimerà J, 1998. On matrix diffusion: formulations, solution methods and qualitative effects. Hydrogeology Journal 6, 178–190.

Chesnut D A, 1994. Dispersivity in heterogeneous permeable media. Report UCRL-JC-114790, Lawrence Livermore National Laboratory, CA.

Crawford J, 2008. Bedrock transport properties Forsmark. Site descriptive modeling, SDM-Site Forsmark. SKB R-08-48, Svensk Kärnbränslehantering AB.

Cvetkovic V, Selroos J-O, Cheng H, 1999. Transport of reactive tracers in rock fractures. Journal of Fluid Mechanics 378, 335–356.

Cvetkovic V, Painter S, Outters N, Selroos J-O, 2004. Stochastic simulation of radionuclide migration in discretely fractured rock near the Äspö Hard Rock Laboratory. Water Resources Research 40, W02404. doi:10.1029/2003WR002655

de Hoog F R, Knight J H, Stokes A N, 1982. An improved method for numerical inversion of Laplace transforms. SIAM Journal on Scientific and Statistical Computing 3, 357–366.

Dershowitz W S, Fidelibus C, 1999. Derivation of equivalent pipe network analogues for three-dimensional discrete fracture networks by boundary element method. Water Resources Research 35, 2685–2691.

Dershowitz W S, Lee G, Geier J, Foxford T, LaPointe P, Thomas A, 1998. FracMan version 2.6 interactive discrete feature data analysis, geometric modeling, and exploration simulation, user documentation. Report 923–1089, Golder Associates Inc, Seattle, WA.

Develi K, Babadagli T, 2015. Experimental and visual analysis of single-phase flow through rough fracture replicas. International Journal of Rock Mechanics and Mining Sciences 73, 139–155.

Follin S, 2008. Bedrock hydrogeology Forsmark. Site descriptive modeling, SDM-Site Forsmark. SKB R-08-95, Svensk Kärnbränslehantering AB.

Gelhar L W, Welty C, Rehfeldt K R, 1992. A critical review of data on field-scale dispersion in aquifer. Water Resources Research 28, 1955–1974.

Gelhar L W, 1993. Stochastic subsurface hydrology. Prentice-Hall.

Gerke H H, van Genuchten M T, 1996. Macroscopic representations of structural geometry for simulating water and solute movement in dual-porosity media. Advances in Water Resources 19, 343–357.

Gylling B, 1997. Development and applications of the channel network model for simulations of flow and solute transport in fractured rock. PhD thesis. Department of Chemical Engineering and Technology, Royal Institute of Technology, Stockholm, Sweden.

Gylling B, Moreno L, Neretnieks I, 1999. The Channel Network Model – A tool for transport simulation in fractured media. Groundwater 37, 367–375.

Hartley L, Roberts D, 2013. Summary of discrete fracture network modeling as applied to hydrogeology of the Forsmark and Laxemar sites. SKB R-12-04, Svensk Kärnbränslehantering AB.

Hollenbeck K J, 1998. INVLAP.m: A MATLAB function for numerical inversion of Laplace transforms by the de Hoog algorithm. Available at: https://www.mathworks.com/matlabcentral/answers/uploaded_files/1034/invlap.m;

Holmén J G, Stigsson M, 2001. Modelling of future hydrogeological conditions at SFR. SKB R-01-02, Svensk Kärnbränslehantering AB.

Huber F, Enzmann F, Wenka A, Bouby M, M Dentz, Schäfer T, 2012. Natural micro-scale heterogeneity induced solute and nanoparticle retardation in fractured crystalline rock. Journal of Contaminant Hydrology 133, 40–52.

Johns R A, Roberts P V, 1991. A solute transport model for channelized flow in a fracture. Water Resources Research 27, 1797–1808.

Joyce S, Simpson T, Hartley L, Applegate D, Hoek J, Jackson P, Swan D, Marsic N, Follin S, 2010. Groundwater flow modelling of periods with temperate climate conditions –Forsmark. SKB R-09-20, Svensk Kärnbränslehantering AB.

Koyama T, Li B, Jiang Y, Jing L, 2009. Numerical modelling of fluid flow tests in a rock fracture with a special algorithm for contact areas. Computers and Geotechnics 36, 291–303.

Mahmoudzadeh B, Liu L, Moreno L, Neretnieks I, 2014. Solute transport in a single fracture involving an arbitrary length decay chain with rock matrix comprising different geological layers. Journal of Contaminant Hydrology 164, 59–71.

Min K-B, J Rutqvist, Tsang C-F, Jing L, 2004. Stress dependent permeability of fractured rock masses a numerical study. International Journal of Rock Mechanics and Mining Sciences 41, 1191–1210.

Molz F, 1981. Water transport in sol plant system: a review. Water Resources Research 17, 1245–1260.

Molz F, 2015. Advection, dispersion, and confusion. Groundwater 53, 348–353.

Moreno L, Neretnieks I, 1991. Fluid and solute transport in a network of channels. SKB TR 91-44, Svensk Kärnbränslehantering AB.

Moreno L, Neretnieks I, 1993. Fluid flow and solute transport in a network of channels. Journal of Contaminant Hydrology 14, 163–192.

Moreno L, Neretnieks I, Eriksen T, 1985. Analysis of some laboratory tracer runs in natural fissures. Water Resources Research 21, 951–958.

Moreno L, Tsang Y W, Tsang C-F, Hale F V, Neretnieks I, 1988. Flow and tracer transport in a single fracture: a stochastic model and its relation to some field observations. Water Resources Research 24, 2033–2048.

Moreno L, Tsang C-F, Tsang Y, Neretnieks I, 1990. Some anomalous features of flow and solute transport arising from fracture aperture variability. Water Resources Research 26, 2377–2391.

Neretnieks I, 1980. Diffusion in the rock matrix: An important factor in radionuclide retardation? Journal of Geophysical Research 85, 4379–4397.

Neretnieks I, 1983. A note on fracture flow dispersion mechanisms in the ground. Water Resources Research 19, 364–370.

Neretnieks I, 1984. Nuclear waste repositories in cystalline rock- an overview of nuclide transport mechanisms. In Murakami T, Ewing R C (eds). Scientific basis for nuclear waste management XVIII: symposium held in Kyoto, Japan, 23–27 October 1994. Pittsburgh, PA: Materials Research Society. (Materials Research Society Symposium Proceedings 353)

Neretnieks I, 2002a. Revisiting the advection–dispersion model – testing an alternative. In Findikakis A N (ed). Proceedings of IAHR Groundwater symposium, Berkeley, California, 25–28 March 2002. Available at: http://www.iaea.org/inis/collection/NCLCollectionStore/_Public/32/056/32056051.pdf

Neretnieks I, 2002b. A stochastic multi-channel model for solute transport- Analysis of tracer transport in fractured rock. Journal of Contaminant Hydrology 55, 175–211.

Neretnieks I, 2006. Channeling with diffusion into stagnant water and into a matrix in series. Water Resources Research 42, W11418. doi:10.1029/2005WR004448

Neretnieks I, Moreno L, 2003. Prediction of some in situ tracer tests with sorbing tracers using independent data. Journal of Contaminant Hydrology 61, 351–360.

Neretnieks I, Eriksen T, Tähtinen P, 1982. Tracer movement in a single fissure in granitic rock: some experimental results and their interpretation. Water Resources Research 18, 849–858.

Neuman S P, 2005. Trends, prospects and challenges in quantifying flow and transport through fractured rocks. Hydrogeology Journal 13, 124–147.

Odén M, Niemi A, Tsang C-F, Öhman J, 2008. Regional channelized transport in fractured media with matrix diffusion and linear sorption. Water Resources Research 44, W02421. doi:10.1029/2006WR005632

Palmquist K, Stanfors R, 1987. The Kymmen power station. TBM tunnel. Hydrogeological mapping and analysis SKB TR 87-26, Svensk Kärnbränslehantering AB.

Rasmuson A, Neretnieks I, 1986. Radionuclide transport in fast channels in crystalline rock. Water Resources Research 22, 1247–1256.

Rhén I, Forsmark T, Hartley L, Jackson P, Roberts D, Swan D, Gylling B, 2008. Hydrogeological conceptualisation and parameterisation, Site descriptive modeling, SDM-Site Laxemar. SKB R-08-78, Svensk Kärnbränslehantering AB.

Sahimi M, 2011. Flow and transport in porous media and fractured rock: from classical methods to modern approaches. Hoboken, NJ: Wiley.

Selroos J-O, Follin S, 2010. SR-Site groundwater flow modeling methodology, setup and results. SKB R-09-22, Svensk Kärnbränslehantering AB.

Selroos J-O, Walker D D, Ström A, Gylling B, Follin S, 2002. Comparison of alternative modeling approaches for groundwater flow in fractured rock. Journal of Hydrology 257, 174–188.

SKB, 2004. RETROCK Project. Treatment of geosphere retention phenomena in safety assessments, Scientific basis of retention processes and their implementation in safety assessment models (WP2). Work package 2 report of the RETROCK concerted action. SKB R-04-48, Svensk Kärnbränslehantering AB.

SKB, 2011. Long-term safety for the final repository for spent nuclear fuel at Forsmark Main report of the SR-Site project. SKB TR-11-01, Svensk Kärnbränslehantering AB.

Stanfors R, 1987. The Bolmen tunnel project. Evaluation of geophysical site investigation methods. SKB TR 87-25, Svensk Kärnbränslehantering AB.

Stober I, Bucher K, 2006. Hydraulic properties of the crystalline basement. Hydrogeology Journal 15, 213–224.

Sudicky E A, Frind E O, 1982. Contaminant transport in fractured porous media: analytical solutions for a system of parallel fractures. Water Resources Research 18, 1634–1642.

Tsang C-F, Neretnieks I, 1998. Flow channeling in heterogeneous fractured rocks. Reviews of Geophysics 26, 275–298.

Tsang Y W, Tsang C F, 1987. Channel model of flow through fractured media. Water Resources Research 23, 467–479.

Tsang Y W, Tsang C F, 1989. Flow channeling in a single fracture as a two-dimensional strongly heterogeneous permeable medium, Water Resources Research 25, 2076–2080.

Tsang Y W, Tsang C F, 2001. A particle-tracking method for advective transport in fractures with diffusion into finite matrix blocks. Water Resources Research 37, 831–835.

Tsang Y W, Tsang C F, Neretnieks I, Moreno L, 1988. Flow and tracer transport in fractured media – A variable-aperture channel model and its properties. Water Resources Research 24, 2049–2060.

Öhberg A, Rouhiainen P, 2000. Posiva groundwater flow measuring techniques. Posiva 2000-12, Posiva Oy, Finland.

Arkitektkopia AB, Bromma, 2017

SKB is responsible for managing spent nuclear fuel and radioactive waste produced by the Swedish nuclear power plants such that man and the environment are protected in the near and distant future.

skb.se